Journal of Computational and Applied Mathematics 234 (2010) 1678–1684

Contents lists available at ScienceDirect

Journal of Computational and Applied Mathematics

journal homepage: www.elsevier.com/locate/cam

Mathematical modeling of seismic and acousto-gravitational waves in a heterogeneous earth–atmosphere model☆

B. Mikhailenko, G. Reshetova *

The Institute of Computational Mathematics and Mathematical Geophysics, pr. Lavrentieva, 6, Novosibirsk, Russia

ARTICLE INFO

Article history:
Received 27 November 2007
Received in revised form 23 March 2009

Keywords:
Numerical techniques
Seismic modeling
Seismic-wave propagation
Seismology

ABSTRACT

A numerical–analytical solution to problems of seismic and acoustic-gravitational wave propagation is applied to a heterogeneous Earth–Atmosphere model. The seismic wave propagation in an elastic half-space is described by a system of first order dynamic equations of the elasticity theory. The propagation of acoustic-gravitational waves in the atmosphere is described by the linearized Navier–Stokes equations. The algorithm proposed is based on the integral Laguerre transform with respect to time, the finite integral Bessel transform along the radial coordinate with a finite difference solution of the reduced problem along the vertical coordinate. The algorithm is numerically tested for the heterogeneous Earth–Atmosphere model for different source locations.

1. Introduction

The problem of the propagation of acoustic-gravitational waves in a heterogeneous atmosphere has long been known. The first publications concerning the impact of the gravitational field on the wave processes in the atmosphere and ocean appeared in the middle of the last century [1]. Martyn [2] and Hines [3] indicated an important role of acoustic-gravitational waves for understanding and interpretation of numerous physical processes in the atmosphere. Starting in the fifties, an increasing interest in studying the generation and propagation of the acoustic-gravitational waves in the real atmosphere is associated with the development of the infrasonic method of monitoring the nuclear explosions in the atmosphere. A review on studying the basic characteristics of the acoustic-gravitational waves in the atmosphere can be found in [4–6].

In many theoretical studies, the Earth–Atmosphere interface is considered to be absolutely reflecting, the effects, related to the excitation of seismic waves in the Earth's crust and their interaction with the acoustic-gravitational waves in the atmosphere being neglected. In the past few decades, theoretical and experimental studies have shown a close relation between the lithospheric and the atmospheric wave motions. In a number of papers (see, for example, [7–10]) the acoustic-seismic induction effect is discussed. Alekseev [11] discovered the effect of acoustic-seismic induction, in which an acoustic wave from a powerful vibrator induced intense surface seismic waves due to the atmospheric refraction at a distance of tens of kilometers.

A specific feature of the numerical modeling of wave fields for a heterogeneous Earth–Atmosphere model is a considerable difference in the velocities of seismic and acoustic waves. In this case, the use of explicit finite difference schemes brings about serious restrictions on the time step of a finite difference scheme and results in large computer costs. Another way of overcoming such difficulties is the application of the frequency-domain modeling. In this case, after employing finite difference (FD) methods with respect to spatial coordinates, we deal with an extremely large matrix to be

☆ Expanded version of a talk presented at the 8th International Conference on Mathematical and Numerical Aspects of Waves (Waves 2007) (Reading, UK, 2007).

* Corresponding author.
E-mail address: kgv@nmsf.sscc.ru (G. Reshetova).

0377-0427/$ – see front matter © 2010 Published by Elsevier B.V.
doi:10.1016/j.cam.2009.08.015

implicitly solved for a great number of temporal frequencies. When simulating the acoustic-gravitational waves propagation in heterogeneous media, this difficulty can be avoided if the Fourier transform with respect to time is replaced by the Laguerre transform. As a result, we obtain a system of algebraic equations, whose matrix is independent of the parameter p—the degree of the Laguerre polynomials. Thus, only the right-hand side of the system has a recurrent dependence on the parameter p. Hence, the system of linear algebraic equations can be solved for a great number of right-hand sides using fast solutions, such as the Cholesky decomposition. Our approach is an analogue to the frequency-domain forward modeling, where instead of the temporal frequency we have the number p—the degree of the Laguerre polynomials. In our paper, we apply the numerical–analytical method to study the wave propagation in a 3D heterogeneous Earth–Atmosphere model with axial symmetry. The algorithm combines the Bessel integral transform along the radial coordinate and the integral Laguerre transform with respect to time with the FD solution along the vertical coordinate. Such an approach has been developed in our previous papers for the problem of seismic wave propagation in the heterogeneous elastic half-space (without taking into account atmosphere at all) in [12,13].

2. Statement of the problem

The system of linearized equations for propagation of acoustic-gravitational waves in a 3D heterogeneous axially symmetric atmosphere in the cylindrical coordinates (r, z) is as follows:

$$\rho_0 \frac{\partial u_z}{\partial t} = -\frac{\partial P}{\partial z} - \rho g, \tag{1}$$

$$\rho_0 \frac{\partial u_r}{\partial t} = -\frac{\partial P}{\partial r}, \tag{2}$$

$$\frac{\partial P}{\partial t} = c_0^2 \left[\frac{\partial \rho}{\partial t} + \frac{\partial \rho_0}{\partial z} u_z \right] - \frac{\partial P_0}{\partial z} u_z, \tag{3}$$

$$\frac{\partial \rho}{\partial t} = -\rho_0 \left[\frac{\partial u_r}{\partial r} + \frac{1}{r} u_r + \frac{\partial u_z}{\partial z} \right] - \frac{\partial \rho_0}{\partial z} u_z + F(r, z, t), \tag{4}$$

where u_r and u_z are the displacement velocity components of air particles in a wave; P and ρ are the pressure and the density perturbations, respectively, under the effect of a mass source in the atmosphere with its distribution given by $F(z, r, t) = \delta(z - z_0) f(t)$, c_0 is the sound velocity in the atmosphere, and g is the acceleration due to gravity. The z-axis is directed upward. Zero in subscripts marks mean values for the unperturbed atmosphere. The dependencies of the atmospheric pressure P_0 and the density ρ_0 on the height are given by $P_0, \rho_0 \sim \exp(-z/H)$, where H is a height of the isothermal homogeneous atmosphere. For the unperturbed atmosphere in a homogeneous gravity field

$$\frac{\partial P_0}{\partial z} = -\rho_0 g; \qquad \rho_0(z) = \rho_1 \exp(-z/H), \tag{5}$$

where ρ_1 is the density at $z = 0$. We assume the Earth–Atmosphere interface to be located at $z = 0$.

The system of first order equations of the elasticity theory for seismic wave propagation in the 3D heterogeneous axially symmetric Earth model in the cylindrical coordinates is as follows:

$$\rho_0 \frac{\partial u_z}{\partial t} = \frac{\partial \sigma_{rz}}{\partial r} + \frac{\partial \sigma_{zz}}{\partial z} + \frac{\sigma_{rz}}{r} + \rho_0 F_z(r, z, t), \tag{6}$$

$$\rho_0 \frac{\partial u_r}{\partial t} = \frac{\partial \sigma_{rr}}{\partial r} + \frac{\partial \sigma_{rz}}{\partial z} + \frac{\sigma_{rr} - \sigma_{\theta\theta}}{r} + \rho_0 F_r(r, z, t), \tag{7}$$

$$\frac{\partial \sigma_{zz}}{\partial t} = (\lambda + 2\mu) \frac{\partial u_z}{\partial z} + \lambda \left(\frac{\partial u_r}{\partial r} + \frac{u_r}{r} \right), \tag{8}$$

$$\frac{\partial \sigma_{rr}}{\partial t} = (\lambda + 2\mu) \frac{\partial u_r}{\partial r} + \lambda \left(\frac{\partial u_r}{\partial z} + \frac{u_r}{r} \right), \tag{9}$$

$$\frac{\partial \sigma_{\theta\theta}}{\partial t} = (\lambda + 2\mu) \frac{u_r}{r} + \lambda \left(\frac{\partial u_z}{\partial z} + \frac{\partial u_r}{\partial r} \right), \tag{10}$$

$$\frac{\partial \sigma_{rz}}{\partial t} = \mu \left(\frac{\partial u_r}{\partial z} + \frac{\partial u_z}{\partial r} \right). \tag{11}$$

In these equations, u_r and u_z are the displacement velocity components in the elastic half-space, $\sigma_{zz}, \sigma_{rr}, \sigma_{rz}, \sigma_{\theta\theta}$ are the stress tensor components, $\rho_0(z)$ is the density of the elastic half-space, and $\lambda(z)$ and $\mu(z)$ are the Lame constants. F_z, F_r

are the components of the force $\vec{F}(z,r,t) = F_z(z,r,t)\vec{e}_z + F_r(z,r,t)\vec{e}_r$ that describe the distribution of an explosive, a vertical-force or a dipole source in the elastic half-space. For an explosive source, they are:

$$F_z(z,r,t) = \frac{\delta(r)}{2\pi r}\frac{\mathrm{d}}{\mathrm{d}z}\delta(z-z_0)f(t), \qquad F_r(z,r,t) = \frac{\mathrm{d}}{\mathrm{d}r}\frac{\delta(r)}{2\pi r}\delta(z-z_0)f(t). \tag{12}$$

The function $f(t)$ is a time-dependent source wavelet. The sources are formally described using equations that include generalized functions and their derivatives. In the numerical solution, the corresponding smooth equivalents of the generalized functions are used. Eqs. (1)–(4) and (6)–(11) are solved at zero initial parameters in the atmosphere

$$u_z|_{t=0} = u_r|_{t=0} = P|_{t=0} = \rho|_{t=0} = 0, \tag{13}$$

and in the elastic half-space

$$u_z|_{t=0} = u_r|_{t=0} = \sigma_{zz}|_{t=0} = \sigma_{rr}|_{t=0} = \sigma_{rz}|_{t=0} = \sigma_{\theta\theta}|_{t=0} = 0, \tag{14}$$

with the fitting condition at the Earth–Atmosphere interface

$$u_z\,|_{z=-0} = u_z\,|_{z=+0}\,; \qquad \left.\frac{\partial\sigma_{zz}}{\partial t}\right|_{z=-0} = -\left.\left(\frac{\partial P}{\partial t} + \frac{\partial P_0}{\partial z}u_z\right)\right|_{z=+0}; \qquad \sigma_{rz}|_{z=-0} = 0. \tag{15}$$

For convenience, we assume that the interface is located at $z = 0$. In the concise notation, Eqs. (1)–(4) and (6)–(11) are written down as a single system

$$\rho_0\frac{\partial u_z}{\partial t} = \frac{\partial\sigma_{rz}}{\partial r} + \frac{\partial\sigma_{zz}}{\partial z} + \frac{\sigma_{rz}}{r} - U\rho g + L\frac{\delta(r)}{2\pi r}\frac{\mathrm{d}}{\mathrm{d}z}\delta(z-z_0)f(t), \tag{16}$$

$$\rho_0\frac{\partial u_r}{\partial t} = \frac{\partial\sigma_{rr}}{\partial r} + \frac{\partial\sigma_{rz}}{\partial z} + \frac{\sigma_{rr}-\sigma_{\theta\theta}}{r} + L\frac{\mathrm{d}}{\mathrm{d}r}\frac{\delta(r)}{2\pi r}\delta(z-z_0)f(t), \tag{17}$$

$$\frac{\partial\sigma_{zz}}{\partial t} = (\lambda+2\mu)\frac{\partial u_z}{\partial z} + \lambda\left(\frac{\partial u_r}{\partial r} + \frac{u_r}{r}\right) - U\rho_0 g u_z - Uc_0^2\delta(z-z_0)f(t), \tag{18}$$

$$\frac{\partial\sigma_{rr}}{\partial t} = (\lambda+2\mu)\frac{\partial u_r}{\partial r} + \lambda\left(\frac{\partial u_r}{\partial z} + \frac{u_r}{r}\right) - U\rho_0 g u_z - Uc_0^2\delta(z-z_0)f(t), \tag{19}$$

$$\frac{\partial\sigma_{\theta\theta}}{\partial t} = (\lambda+2\mu)\frac{u_r}{r} + \lambda\left(\frac{\partial u_z}{\partial z} + \frac{\partial u_r}{\partial r}\right) - U\rho_0 g u_z - Uc_0^2\delta(z-z_0)f(t), \tag{20}$$

$$\frac{\partial\sigma_{rz}}{\partial t} = \mu\left(\frac{\partial u_r}{\partial z} + \frac{\partial u_z}{\partial r}\right), \tag{21}$$

$$U\left[\frac{\partial\rho}{\partial t} = -\rho_0\left(\frac{\partial u_r}{\partial r} + \frac{u_r}{r} + \frac{\partial u_z}{\partial z}\right) - \frac{\partial\rho_0}{\partial z}u_z + \delta(z-z_0)f(t)\right]. \tag{22}$$

System (1)–(4) for the atmosphere is derived from (16)–(22) assuming

$$\sigma_{rr} = \sigma_{zz} = \sigma_{\theta\theta} = -P; \quad \mu = 0; \quad \lambda = c_0^2\rho_0; \quad \sigma_{rz} = 0; \quad L = 0; \quad U = 1.$$

System (6)–(11) for the elastic half-space is recovered from (16)–(22) assuming that $L = 1$, $U = 0$. In this case, Eq. (22) is formally multiplied by zero, thus it is not taken into consideration. The conditions at the interface for $z = 0$ are given by

$$u_z|_{z=-0} = u_z|_{z=+0}; \qquad \left.\frac{\partial\sigma_{zz}}{\partial t}\right|_{z=-0} = \left.\left(\frac{\partial\sigma_{zz}}{\partial t} + \rho_0 g u_z\right)\right|_{z=+0}; \qquad \sigma_{rz}|_{z=-0} = 0. \tag{23}$$

3. The solution algorithm

The solution of (16)–(22) is searching by separation of the radial variable. This separation is performed by means of Fourier–Bessel integral transformation with respect to r over some finite interval $(0, a)$. Its length is chosen large enough in order to avoid reflections coming back before desired time T. So, at the first step, we obtain a solution to (16)–(22), with zero initial data and boundary conditions (23), as the Fourier–Bessel series

$$\begin{pmatrix} u_r \\ \sigma_{rz} \end{pmatrix} = \frac{2}{a^2}\sum_{n=1}^{\infty}\begin{pmatrix} \bar{u}_r \\ \bar{\sigma}_{rz} \end{pmatrix}\frac{J_1(k_n r)}{(J_0(k_n a))^2}, \tag{24}$$

$$\begin{pmatrix} u_z \\ \sigma_{zz} \\ \rho \end{pmatrix} = \frac{2}{a^2}\sum_{n=1}^{\infty}\begin{pmatrix} \bar{u}_z \\ \bar{\sigma}_{zz} \\ Q_3 \end{pmatrix}\frac{J_0(k_n r)}{(J_0(k_n a))^2}, \tag{25}$$

$$\sigma_{rr} = \frac{2}{a^2}\sum_{n=1}^{\infty}(k_nQ_1 + Q_2)\frac{J_0(k_nr)}{(J_0(k_na))^2} - \frac{2}{a^2}\sum_{n=1}^{\infty}\frac{1}{r}Q_1\frac{J_1(k_nr)}{(J_0(k_na))^2}, \tag{26}$$

$$\sigma_{\theta\theta} = \frac{2}{a^2}\sum_{n=1}^{\infty}\frac{1}{r}Q_1\frac{J_1(k_nr)}{(J_0(k_na))^2} + \frac{2}{a^2}\sum_{n=1}^{\infty}Q_2\frac{J_0(k_nr)}{(J_0(k_na))^2}, \tag{27}$$

where k_n are the roots of the equation $J_1(k_na) = 0$. The coefficients $\bar{u}_z, \bar{u}_r, \bar{\sigma}_{rz}, \bar{\sigma}_{zz}, \bar{\sigma}_{rr}, \bar{\sigma}_{\theta\theta}, Q_1, Q_2, Q_3$ in (24)–(27) are functions of (n, z, t). After the Bessel transform, we obtain

$$\frac{\partial\bar{u}_z}{\partial t} - \frac{1}{\rho_0}\frac{\partial\bar{\sigma}_{zz}}{\partial z} - \frac{k_n}{\rho_0}\bar{\sigma}_{rz} + U\frac{g}{\rho_0}Q_3 = L\frac{1}{2\pi}\frac{\mathrm{d}}{\mathrm{d}z}\delta(z - z_0)f(t), \tag{28}$$

$$\frac{\partial\bar{u}_r}{\partial t} - \frac{1}{\rho_0}\frac{\partial\bar{\sigma}_{rz}}{\partial z} + \frac{k_n}{\rho_0}(k_nQ_1 + Q_2) = -L\frac{1}{2\pi}k_n\delta(z - z_0)f(t), \tag{29}$$

$$\frac{\partial\bar{\sigma}_{zz}}{\partial t} - \rho_0c_p^2\frac{\partial\bar{u}_z}{\partial z} - k_n\rho_0\left(c_p^2 - 2c_s^2\right)\bar{u}_r + U\rho_0g\bar{u}_z = -Uc_0^2\delta(z - z_0)f(t), \tag{30}$$

$$\frac{\partial\bar{\sigma}_{rz}}{\partial t} - \rho_0c_s^2\frac{\partial\bar{u}_r}{\partial z} + k_n\rho_0c_s^2\bar{u}_z = 0, \tag{31}$$

$$\frac{\partial Q_1}{\partial t} - 2\rho_0c_s^2\bar{u}_r = 0, \tag{32}$$

$$\frac{\partial Q_2}{\partial t} - \rho_0\left(c_p^2 - 2c_s^2\right)\left(\frac{\partial\bar{u}_z}{\partial z} - k_n\bar{u}_r\right) + U\rho_0g\bar{u}_z = -Uc_0^2\delta(z - z_0)f(t), \tag{33}$$

$$\frac{\partial Q_3}{\partial t} + \frac{1}{\left(c_p^2 - 2c_s^2\right)}\frac{\partial Q_2}{\partial t} + \frac{\rho_0g}{\left(c_p^2 - 2c_s^2\right)}\bar{u}_z + \frac{\partial\rho_0}{\partial z}\bar{u}_z = 0. \tag{34}$$

The last equation for Q_3 is derived from the original one

$$\frac{\partial Q_3}{\partial t} = -\rho_0\left(\frac{\partial\bar{u}_z}{\partial z} + k_n\bar{u}_r\right) - \frac{\partial\rho_0}{\partial t}\bar{u}_z + U\delta(z - z_0)f(t) = 0. \tag{35}$$

In these equations, we denote $c_p^2 = (\lambda + 2\mu)/\rho_0$, $c_s^2 = \mu/\rho_0$.

The conditions at the interface become as follows:

$$\bar{u}_z|_{z=-0} = \bar{u}_z|_{z=+0}; \qquad \left.\frac{\partial\bar{\sigma}_{zz}}{\partial t}\right|_{z=-0} = \left.\left(\frac{\partial\bar{\sigma}_{zz}}{\partial t} + \rho_0g\bar{u}_z\right)\right|_{z=+0}; \qquad \bar{\sigma}_{rz}|_{z=-0} = 0. \tag{36}$$

At the second step, we use the integral Laguerre transform. Here we use its modified version in the following form:

$$\tilde{U}^p(n, z, p) = \int_0^{\infty}(ht)^{-\frac{\alpha}{2}}l_p^{\alpha}(ht)\bar{U}(n, z, t)\mathrm{d}(ht), \quad p = 0, 1, 2, \ldots \tag{37}$$

with the inversion formula

$$\bar{U}(n, z, t) = (ht)^{\frac{\alpha}{2}}\sum_{p=0}^{\infty}\frac{p!}{(p + \alpha)!}l_p^{\alpha}(ht)\tilde{U}^p(n, z, p), \tag{38}$$

where $\bar{U}(n, z, t) = (\bar{u}_r, \bar{u}_z, \bar{\sigma}_{zz}, \bar{\sigma}_{rz}, Q_1, Q_2, Q_3)^{\mathrm{T}}$, $\tilde{U}(n, z, p) = (\tilde{u}_r^p, \tilde{u}_z^p, \tilde{\sigma}_{zz}^p, \tilde{\sigma}_{rz}^p, \tilde{Q}_1^p, \tilde{Q}_2^p, \tilde{Q}_3^p)^{\mathrm{T}}$ and the functions $l_p^{\alpha}(t)$ are the orthogonal Laguerre functions:

$$l_p^{\alpha}(ht) = (ht)^{\frac{\alpha}{2}}\,\mathrm{e}^{-\frac{ht}{2}}L_p^{\alpha}(ht). \tag{39}$$

Here we select an integer parameter $\alpha \geq 1$ to satisfy the initial data and introduce a shift parameter $h > 0$. The value of the latter affects the accuracy of the numerical implementation of the algorithm. After the Laguerre transform, we have the system of equations, where the superscript p in $\tilde{u}_r^p, \tilde{u}_z^p, \tilde{\sigma}_{zz}^p, \ldots$ is omitted:

$$\frac{h}{2}\tilde{u}_z - \frac{1}{\rho_0}\frac{\partial\tilde{\sigma}_{zz}}{\partial z} - \frac{k_n}{\rho_0}\tilde{\sigma}_{rz} + U\frac{g}{\rho_0}\tilde{Q}_3 = L\frac{1}{2\pi}\frac{\mathrm{d}}{\mathrm{d}z}\delta(z - z_0)f_p - h\sum_{j=0}^{p-1}\tilde{u}_z^j, \tag{40}$$

$$\frac{h}{2}\tilde{u}_r - \frac{1}{\rho_0}\frac{\partial\tilde{\sigma}_{rz}}{\partial z} - \frac{k_n}{\rho_0}\left(k_n\tilde{Q}_1 + \tilde{Q}_2\right) = -L\frac{1}{2\pi}k_n\delta(z - z_0)f_p - h\sum_{j=0}^{p-1}\tilde{u}_r^j, \tag{41}$$

$$\frac{h}{2}\tilde{\sigma}_{zz} - \rho_0 c_p^2 \frac{\partial \tilde{u}_z}{\partial z} - k_n \rho_0 \left(c_p^2 - 2c_s^2\right) \tilde{u}_r + U\rho_0 g \tilde{u}_z = F - h\sum_{j=0}^{p-1} \tilde{\sigma}_{zz}^j, \tag{42}$$

$$\frac{h}{2}\tilde{\sigma}_{rz} - \rho_0 c_s^2 \frac{\partial \tilde{u}_r}{\partial z} + k_n \rho_0 c_s^2 \tilde{u}_z = -h\sum_{j=0}^{p-1} \tilde{\sigma}_{rz}^j, \tag{43}$$

$$\frac{h}{2}\tilde{Q}_1 - 2\rho_0 c_s^2 \tilde{u}_r = -h\sum_{j=0}^{p-1} \tilde{Q}_1^j, \tag{44}$$

$$\frac{h}{2}\tilde{Q}_2 - \rho_0 \left(c_p^2 - 2c_s^2\right) \left(\frac{\partial \tilde{u}_z}{\partial z} - k_n \tilde{u}_r\right) + U\rho_0 g \tilde{u}_z = F - h\sum_{j=0}^{p-1} \tilde{Q}_2^j, \tag{45}$$

$$\frac{h}{2}\tilde{Q}_3 + \frac{h}{2}\frac{1}{\left(c_p^2 - 2c_s^2\right)}\tilde{Q}_2 + \frac{g\rho_0}{\left(c_p^2 - 2c_s^2\right)}\tilde{u}_z + \frac{\partial \rho_0}{\partial z}\tilde{u}_z = -h\sum_{j=0}^{p-1} \left(\tilde{Q}_3^j + \frac{1}{\left(c_p^2 - 2c_s^2\right)}\tilde{Q}_2^j\right), \tag{46}$$

where $F = -Uc_0^2\delta(z - z_0)f_p$ and f_p is the coefficient of the Laguerre series of the source function $f(t)$. The coefficients $\tilde{u}_z$, $\tilde{u}_r$, $\tilde{\sigma}_{rz}$, $\tilde{\sigma}_{zz}$, $\tilde{\sigma}_{rr}$, $\tilde{\sigma}_{\theta\theta}$, $\tilde{Q}_1$, $\tilde{Q}_2$, $\tilde{Q}_3$ in (40)–(46) are the functions of (n, z, p). After applying the Laguerre transform, the conditions at the interface $z = 0$ become as follows:

$$\begin{aligned} &\tilde{u}_z\big|_{z=-0} = \tilde{u}_z\big|_{z=+0}; \qquad \tilde{\sigma}_{rz}|_{z=-0} = 0. \\ &\left(\frac{h}{2}\tilde{\sigma}_{zz} + h\sum_{j=0}^{p-1} \tilde{\sigma}_{zz}^j\right)\Bigg|_{z=-0} = \left(\frac{h}{2}\tilde{\sigma}_{zz} + h\sum_{j=0}^{p-1} \tilde{\sigma}_{zz}^j + \rho_0 g \tilde{u}_z\right)\Bigg|_{z=+0}. \end{aligned} \tag{47}$$

The FD for the system of linear differential equations (40)–(47) with respect to z was applied using the staggered grids [14] providing second order accuracy approximation. This scheme is used within the computation domains in the atmosphere and in the elastic half-space, the fitting conditions at the interface being exactly satisfied. Note that only the right-hand side of this system of ODE includes the parameter p (the degree of the Laguerre polynomials) and has a recurrent p dependence. The matrix is thus independent of p, which makes applicable the fast solutions using the Cholesky decomposition. We decomposed the matrix into the upper and the lower triangular matrices, which gave us a banded matrix with banded components. Thus, we solve (40)–(46) simultaneously for many right-hand sides, or for many p, and then sum up the solutions using inversion (38). The computation repeats for different roots k_n of the Bessel equation to return to the displacement, pressure, and stress components using series (24)–(27). Note that (24)–(27) and (38) exponentially converge with increasing k_n and p, and thus errors associated with the series truncation can be controlled. In our experiments, the error was an order of magnitude lower than that in the FD approximation of derivatives along z in (40)–(46).

Our modeling case is particular as we simulate the wave motion together in the atmosphere and in the elastic Earth. Waves in the atmosphere being 10–15 times slower than in the elastic half-space, the processes have to be considered over long time intervals and, hence, over large spatial domains. The computation domains in the atmosphere and in the elastic Earth are constrained in the vertical direction by introducing Perfectly Matched Layers (PML) [15]. In this study, we adapt the PML algorithm, which was originally designed for solving non-stationary problems, to the equation systems for the atmosphere and an elastic half-space that follow the integral Laguerre transform along the time coordinate. Unlike the time-domain application of the PML method, we achieved stable solutions for quite narrow absorbing layers (narrower than a wavelength) without increasing the computation time. For a more detailed description of such a version of the PML algorithm for the elasticity equation system, see [16].

4. Numerical examples

To gain a better understanding of the wave propagation in the Earth and in the atmosphere, we begin with simple homogeneous models of an elastic half-space that borders on the atmosphere, where the sound velocity is constant but density decreases exponentially with height. The wave propagation velocities in the elastic half-space are $v_p = 3000$ m/s, $v_s = 1760$ m/s and the density is $\rho_0 = 2300$ kg/m^3. The velocity of acoustic waves in the atmosphere is $c_0 = 340$ m/s and the density is $\rho_0 = 1.225$ kg/m^3 (at $z = 0$).

Fig. 1(left) shows computed snapshots at the time $t = 20$ s for the component u_r in the elastic half-space and in the atmosphere. The explosive source located in the elastic half-space at a depth of $z = 3000$ m (1λ, where λ is the dominant wavelength of the P-wave in the elastic Earth), generates a direct P-wave and a PP-wave reflected from the Earth–Atmosphere interface, and then a converted PS-wave; a conical wave propagating in the atmosphere. The wavefield becomes more complex if an explosive source is located nearer to the free surface at a depth of 750 m ($1/4\lambda$). In this case, a non-geometric wave S^* appears in the elastic half-space in addition to the classical P–PP and P–PS waves, Fig. 1(right). The S^*-wave related to a heterogeneous plane P-wave in the source attenuates exponentially with distance. Its contribution

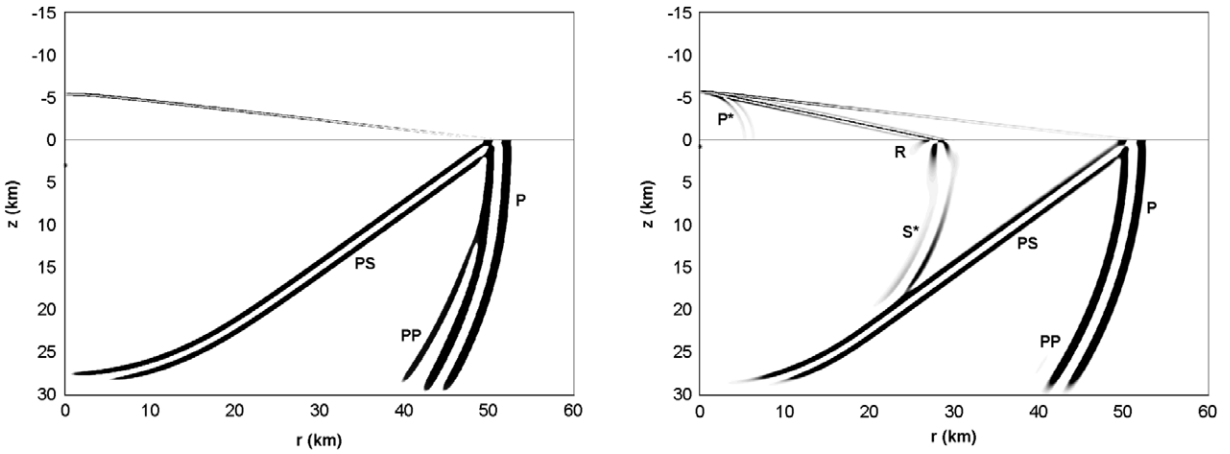

Fig. 1. Computed snapshots at the time $t = 20$ s for the component u_r in the elastic half-space and atmosphere with source positions 1λ (left) and $1/4\lambda$ (right).

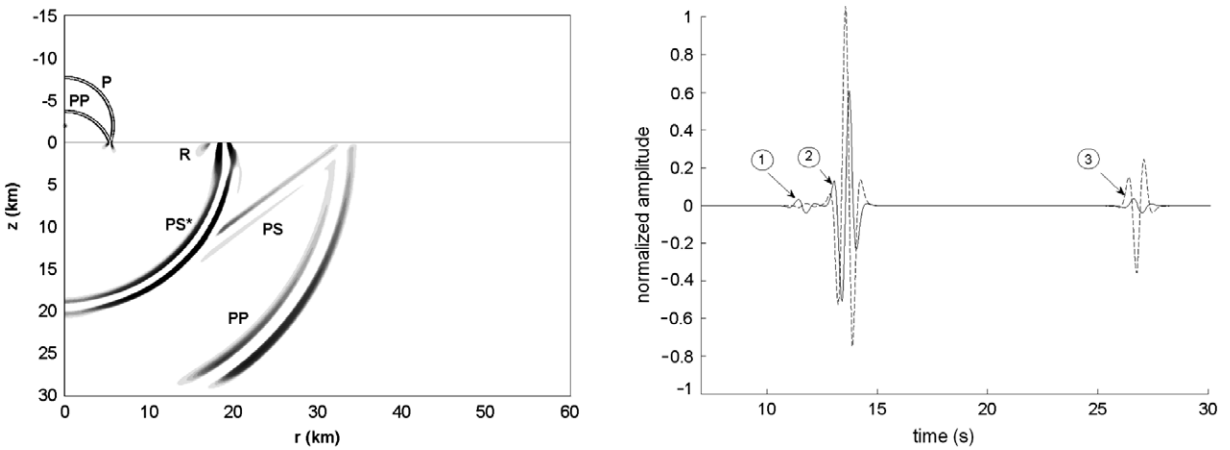

Fig. 2. A snapshot at the time $t = 20$ s for u_r component for a source, located in the atmosphere at a height of 2 km (left); computed seismograms for u_z (dashed) and u_r (solid) components at the Earth–Atmosphere interface (right).

to the wave field is considerable at a distance shorter than a wavelength (see e.g. [17]). In its own turn it generates a non-geometric *P*-wave in the atmosphere. The snapshot also includes a Stoneley surface wave propagating along the Earth–Atmosphere interface and conical waves in the atmosphere. It is worth pointing out that the Fourier–Bessel transform with respect to radial variable r and application of Laguerre decomposition with respect to time leads to a split system of ODE, that is to a series of 1D problems. For its numerical solution, an extremely fine spatial grid can be used in order to provide a reliable simulation of Stonely and acoustic waves. A snapshot at the time $t = 20$ s for the component u_r in the elastic half-space and in the atmosphere for the model with the same parameters as above, for a source, located in the atmosphere at a height of 2 km (about 6λ, where λ is the dominant wavelength in the atmosphere) is presented in Fig. 2(left). One can observe intense heterogeneous plane waves, even at this distance between the source and the Earth–Atmosphere interface. The reason is that an exponential amplitude decrease of these waves depends on distance as well as on the medium parameters included in the exponent. Note that the atmospheric density is over 1000 times lower than that of the elastic Earth. The snapshot shows a non-geometric PS^* wave in addition to the refracted *P* and *PS* waves. The non-geometric wave is produced by the interaction of heterogeneous plane *P* waves with an elastic subsurface over the source. Waves in the atmosphere are a direct *P* wave from the source and a *PP* reflection from the Earth–Atmosphere interface. Fig. 2(right) shows the vertical and horizontal displacement components at the Earth–Atmosphere interface. The first arrivals (1) are of a *P* head wave in the elastic half-space, the second one (2) is a Stoneley wave, and (3) is an acoustic wave. Note that the acoustic wave incident to the elastic half-space shows an elliptic polarization, possibly because the Earth–Atmosphere interface is a creeping interface.

Consider a numerical example illustrating the case of a high-frequency seismic exploration bandwidth and a model of an explosive source in the atmosphere 10 m above the Earth–Atmosphere interface with a dominant frequency of $f_0 = 20$ Hz. Let us introduce into the above model an elastic 20 m thin layer that bounds the atmosphere with wave propagation

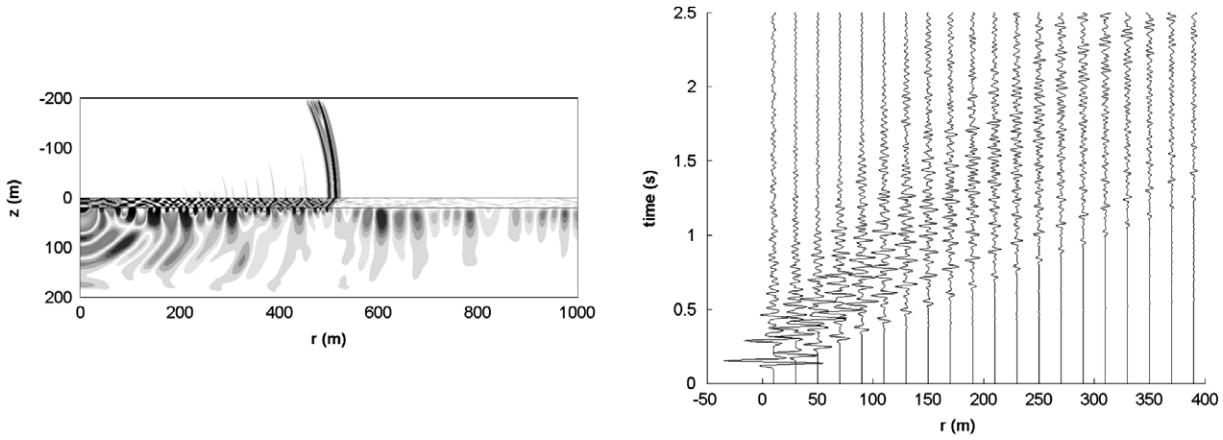

Fig. 3. A snapshot at the time $t = 2.5$ s for u_z component (left); computed seismogram for u_z at the Earth–Atmosphere interface (right).

velocities being lower than in the atmosphere: $v_P = 250$ m/s, $c_s = 150$ m/s, and $\rho_0 = 1700$ kg/m^3. This case is common for seismic exploration in the presence of a low-velocity zone. A snapshot Fig. 3(left) at the time $t = 2.5$ s for the component u_z images non-geometric waves PP^*, PS^* and conical P, S waves in the elastic half-space. Fig. 3(right) shows synthetic seismograms of the displacement velocity at the Earth–Atmosphere interface.

5. Conclusions

We offer a numerical–analytical algorithm applied to simulate the propagation of seismic and acoustic-gravitational waves within the limits of a heterogeneous Earth–Atmosphere model. The algorithm proposed is based on the integral Laguerre transform with respect to time, the finite integral Bessel transform along the radial coordinate with the finite difference solution of the reduced problem along the vertical coordinate. The algorithm is numerically tested for simple models.

Acknowledgements

The first and second authors were supported by the Russian Foundation for Basic Research, grants 06-05-64149, 07-05-00538.

References

[1] H. Lamb, Hydrodynamics, Dover Publications, New York, 1945, p. 541.
[2] D.F. Martyn, Cellular atmospheric waves, Proc. R. Soc. London A201 (1950) 216–234.
[3] C.O. Hines, Internal atmospheric gravity waves at ionospheric heights, Can. J. Phys. 38 (1960) 1441–1481.
[4] S.H. Francis, Global propagation of atmospheric gravity waves: A review, J. Atmos. Terr. Phys. 37 (1975) 1011–1054.
[5] E.E. Gossard, W.H. Hooken, Waves in the Atmosphere, Elsevier Scientific Publishing Company, 1975, p. 532.
[6] G.I. Grigoriev, Acoustic-gravitational waves in the Earth's atmosphere (review), Izv. Vyzov Radiofiz. XLII (1) (1999) 3–25.
[7] J. Artru, P. Lognonne et E. Blanc, Normal modes modeling of post-seismic ionospheric oscillations, Geophys. Res. Lett. 28 (2001) 697–700.
[8] N. Kobayashi, A new method to calculate normal modes, Geophys. J. Int. 168 (2006) 315–331.
[9] P. Lognonne, C. Clevede, H. Kanamori, Normal mode summation of seismograms and barograms in an spherical earth with realistic atmosphere, Geophys. J. Int. 135 (1998) 388–406.
[10] S. Watada, Part I: Near–source acoustic coupling between the atmosphere and the solid earth during volcanic eruptions. Part II: Nearfield normal mode amplitude anomalies of the landers earthquake, Ph.D. Thesis at: http://adsabs.harvard.edu/abs/1995PhDT.....46W.
[11] A.S. Alekseev, B.M. Glinsky, S. Dryakhlov, The effect of acoustic-seismic induction in vibroseismic soundings, Dokl. RAN 346 (5) (1996) 664–667 (in Russian).
[12] G.V. Konyukh, B.G. Mikhailenko, Application of the Laguerre integral transform for solving dynamic seismic problems, Bull. Novosibirsk Comput. Center. Ser. Math. Model. Geophys. 4 (1998) 79–91.
[13] B.G. Mikhailenko, A.A. Mikhailov, G.V. Reshetova, Numerical modeling of transient seismic fields in viscoelastic media based on the Laguerre spectral method, Pure Appl. Geophys. 160 (2003) 1207–1224.
[14] J. Virieux, *P*-, *SV*-wave propagation in heterogeneous media: Velocity–stress finite-difference method, Geophysics 51 (4) (1986) 889–901.
[15] J.P. Berenger, A perfectly matched layer for the absorption of electromagnetic waves, J. Comput. Phys. 114 (1994) 185–200.
[16] G.V. Reshetova, V.A. Tcheverda, Nonsplit PML on the base of Laguerre transformation, Mat. Model. 18 (9) (2006) 91–101.
[17] M. Roth, K. Holliger, The non-geometric, *P*- and *S*-wave in high-resolution seismic data: Observations and modeling, Geophys. J. Int. 140 (2000) F5–F11.